**THE EUROPEAN
PHYSICAL JOURNAL D**

Regular Article

Absolute OH density determination by laser induced fluorescence spectroscopy in an atmospheric pressure RF plasma jet

Q. Xiong[1,2], A.Yu. Nikiforov[2,3,a], L. Li[2], P. Vanraes[2], N. Britun[4], R. Snyders[4,5], X.P. Lu[1], and C. Leys[2]

[1] College of Electrical and Electronic Engineering, HuaZhong University of Science and Technology, WuHan, Hubei 430074, P.R. China
[2] Department of Applied Physics, Research Unit Plasma Technology, Ghent University, Sint-Pietersnieuwstraat 41, B4, 9000 Ghent, Belgium
[3] Institute of Solution Chemistry of the Russian Academy of Science, Academicheskaya St., 1, Ivanono, 153045, Russia
[4] Chimie des Interactions Plasma-Surface (ChIPS), CIRMAP, Université de Mons, 20 place du Parc, 7000 Mons, Belgium
[5] Materia Nova Research Center, Parc Initialis, 7000 Mons, Belgium

Abstract. In this paper, the ground state OH density is measured in high pressure plasma by laser-induced fluorescence (LIF) spectroscopy. The OH density determination is based on the simulation of the intensity fraction of fluorescence from the laser-excited level of OH (A) in the total detected LIF signal. The validity of this approach is verified in an atmospheric pressure Ar + H_2O plasma jet sustained by a 13.56 MHz power supply. The transition line $P_1(4)$ from $OH(A, v' = 1, J' = 3) \rightarrow OH(X, v'' = 0, J'' = 4)$ is used for the LIF excitation. The absolute OH density is determined to be 2.5×10^{19} m^{-3} at 1 mm away from the jet nozzle. It corresponds to a dissociation of 0.06% of the water vapor in the working gas. Different mechanisms of OH (X) production in the core of the plasma jet are discussed and analyzed.

1 Introduction

The hydroxyl radical (OH) is one of the most important reactive species in plasma chemistry due to its high oxidization feature. Chemical reactions with OH initiate destruction of harmful components like carbon monoxide (CO), volatile organic compounds (VOCs) and methane (CH_4), which is of a primary importance in plasma treatments on exhaust gases [1,2]. OH is also an essential chemical intermediate occurring in combustion environments. It is one of the components necessary for formation of H_2O_2, which is reported as an important high reactive species in water treatment by plasmas [3–5]. Determination of the absolute density of OH radicals is of special interest, due to its important role in plasma chemistry. However, most common passive diagnostic techniques, such as optical emission spectroscopy (OES), fail to give reliable quantitative information on the ground state OH species. In this case, advanced laser active diagnostics, i.e. laser induced fluorescence (LIF) spectroscopy, is desirable [6,7]. The narrow spectral line width of the laser permits the specific selection of species and their level of excitation. LIF diagnostics gives access to the measurement of the spatial and temporal distribution of the species densities as function of the discharge parameters. In its basic principle, LIF implies one photon excites the studied species from

the ground state to an excited state, followed by spontaneous emission (fluorescence) of a photon by decay back to the ground or an intermediate state [8]. The single-point and 2-D laser-induced fluorescence of the OH $A^2\Sigma^+$–$X^2\Pi$ band system has been applied to the study of OH (X) in different kinds of atmospheric plasma. The determination of the local OH concentration or the velocity distribution of laser induced OH (A) relies upon a proportionality between the fluorescence intensity and the concentration of the OH radical in the lower laser-coupled energy level. The quantity of fluorescence reflects the fraction of molecules promoted to the excited state which undergo radiative decay back to the ground stare. It is influenced by a number of factors, including the rates for spontaneous emission and for collisional energy transfer processes such as quenching, vibrational energy transfer (VET) and rotational energy transfer (RET). In molecular LIF experiments, the observed fluorescence is thus comprised of different spectral emissions from different excited levels due to the VET and RET processes induced by collisions with the surrounding species. The spontaneous transitions from the laser excited level of OH ($A^2\Sigma^+$) compete with these fast processes which transfer the molecule to a different rotational state within the same vibrational manifold (rotational energy transfer, RET) or to a different vibrational level (vibrational energy transfer, VET) and these processes result in the generation of additional ro-vibrational

[a] e-mail: anton.nikiforov@ugent.be

emission bands in the LIF spectrum [9–12]. Therefore, a complex function of pressure, temperature, chemical composition and the distribution of OH molecules throughout the large manifold of ro-vibronic energy levels determine the detected broadband LIF signal. Efficiency of VET and RET processes can be controlled in low pressure plasmas by variation of the collider densities. However, these processes have to be considered in high pressure plasmas and obviously cannot be neglected in atmospheric pressure discharges sustained in recombination regime. One of the first published works on the detection of hydroxyl radicals in high-pressure discharges using LIF was made by Ershov and Borysow [10], in which the author employed the time-resolved fluorescence from (0,0) emission at 309 nm after (0,1) excitation at 282 nm to clarify the dynamics of the OH ground state during the pulsed discharge. Ono and Oda measured the absolute OH density and the gas temperature in a pulsed positive corona discharge using predissociation fluorescence (LIPF) with (0,3) excitation around 247 nm [11]. The OH fluorescence directly from laser coupled excited level ($A^2\Sigma^+$, $v' = 3$) to ($X^2\Pi$, $v'' = 2$) was used for the calculation of the absolute OH density. Although the spontaneous de-excitation probabilities of the excited energy level has been taken into account in their three level model, the high rate of predissociation and ignoring additional ro-vibrational emission due to RET process may result in the underestimation of the real OH density. In their recent research, a modified method is proposed for determination of the absolute density of OH radicals in an atmospheric pressure helium plasma jet [12]. After excitation (0,1) from the ground level by 283 nm irradiation, both the fluorescence from the $A^2\Sigma^+$ ($v' = 1$)–$X^2\Pi$ ($v'' = 1$) band at 315 nm and the $A^2\Sigma^+$ ($v' = 0$)–$X^2\Pi$ ($v'' = 0$) band at 309 nm is measured. Another method of comparison between the known reaction rates of the most important loss processes of OH and the time-dependent LIF intensity can give an estimation of the absolute OH density only in pulsed discharge [13,14]. The gas temperature is also obtained by excitation LIF. With this method, the rotational temperature of the ground state of OH is measured in pulsed filamentary discharge, generated in a pin-to-pin geometry [15]. This temperature is equal to the gas temperature only when the characteristic time for RET is much shorter than the lifetime of OH ($A^2\Sigma^+$, $v' = 0, 1$). A typical scheme of the process in LIF measurements of OH is presented in Figure 1, in which the important quenching and pre-dissociation processes are included as well.

All these competing processes induce an impact on the LIF production and change the ro-vibrational population distribution of OH (A) and modify the spectral and temporal shape of the fluorescence signal, which finally leads a complicated interpretation of the experimental results. Therefore, both an approximation according to which the detected LIF signal originates from a single upper ro-vibrational level and an estimation of the OH density by fitting the LIF signal decay with consideration of only a quenching mechanism are inaccurate for the concentration determination of OH radicals [15,16]. In this work,
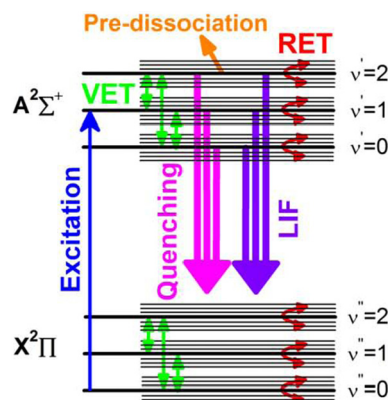

Fig. 1. (Color online) Typical scheme of different competing processes in LIF measurements of hydroxyl radicals.
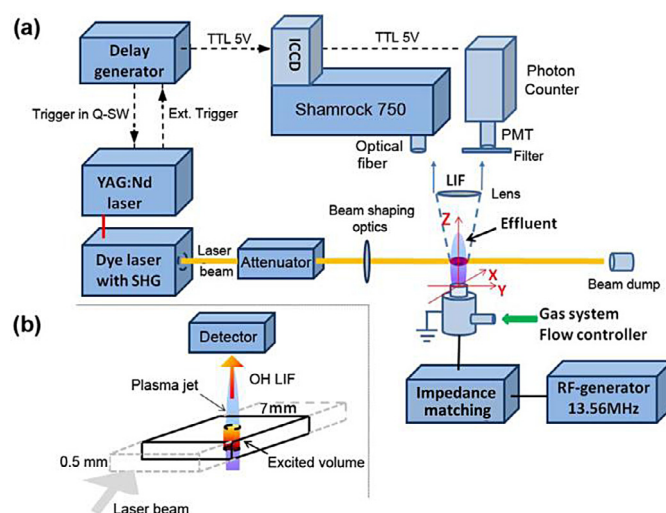

Fig. 2. (Color online) (a) Schematics of the LIF signal and spectra detection systems and the RF plasma jet. (b) Optical arrangement of the LIF detection of OH radicals with the geometric dimension of the laser slice.

an improved calculation model for the ground state OH density determination is proposed, based on LIF diagnostic measurements, in which the effects of fast RET, VET and quenching mechanisms are considered and the LIF spectrum is simulated for fitting the experimental data. Calibration of the LIF signal is performed by Rayleigh scattering on air molecules in open air.

2 Experimental set-up

The experimental arrangement utilized in the measurements is shown in Figure 2.

The plasma jet, which consists of a tungsten electrode in the quartz tube, was connected to a radio-frequency (RF) power supply through a L-matching network and mounted on an optical table in front of a laser. The laser output beam was extended into a slice with a cross section of 0.5×7 mm^2 by a cylindrical lens and passing through

the plasma jet. An excitation wavelength of 283.463 nm of the transition $P_1(4)$ from $OH(A, v' = 1, j' = 3)$ to $OH(X, v'' = 0, j'' = 4)$ was used for the LIF measurements in this work. The LIF signal was focused by a cylindrical lens and detected by a Hamamatsu R928 photomultiplier tube (PMT) through a band-pass interference filter ($\lambda_0 = 308$ nm, FWHM = 10 nm). The LIF signal from the PMT was collected by a SR430 photon counter, synchronized with the YAG:Nd laser and accumulated with 1000 pulses. The same experimental arrangements were used to detect the Rayleigh scattering in air in open space during the same measurements. In this case, the values of the collection efficiency η_c and the detection solid angle Ω are considered the same for both the LIF and the Rayleigh scattering measurements. During the Rayleigh scattering measurements, both the plasma and the gas flow were switched off. LIF spectra were collected using an optical fiber mounted perpendicularly to the laser beam at a position 3 cm away from the plasma. The fiber guides the LIF signal to a spectrometer with an intensified charge coupled device (ICCD) camera system (see Fig. 2). The internal digital delay generator (DDG) of the ICCD was synchronised with the pumping laser by using a Standford DG445 DDG having a total time jitter of about 1 ns. The other experimental conditions are listed in Table 1.

The linearity of the LIF signal vs. laser energy (E_{las}) has been verified and the signal was acquired in the linear regime for E_{las}.

3 LIF model of OH radicals excitation

The goal of the present work is to develop a simple model of LIF processes taking into account the importance of the VET and RET mechanisms in the fluorescence signal of OH radicals generated in high pressure plasmas. The model requires knowledge of the fluorescence fraction from the laser-excited level in the measured wavelength-integrated LIF intensity. This value can be calculated or in our case it has been obtained from LIF spectrum simulation by LASKIN [18]. LASKIN is a computer program developed by Rahmann et al. [18] and Kienle et al. [9,19] for simulation of the population dynamics in the $OH(A^2\Sigma^+)$ and $CH(A^2\Delta)$ excited states for linear LIF diagnostics. Unfortunately, the LASKIN program cannot provide the absolute density of the OH radical and has a number of limitations in case of excitation of the vibrational levels different from $OH(A, v' = 0)$ [9]. Based on spectrum simulation, the fluorescence fraction from a specific laser-excited level back to the level of the ground state in the total LIF intensity has been obtained and used in a series of rate equations for the density calculation of the ground state OH species.

In principle, the detected time-integrated LIF intensity I_f from spontaneous $OH(A \rightarrow X)$ transitions can be defined by

$$I_f = \int_0^t I_f dt = \eta_c \Omega_f V_f \sum \left[t(\lambda_{ij}) G(\lambda_{ij}) \int_0^t \varepsilon_{ij}(t)\, dt \right] \tag{1}$$

Table 1. Experimental conditions applied in the LIF measurements of OH radical in the RF jet.

Experimental conditions	Value/descriptions
Discharge RF frequency	13.56 MHz
Averaged RF power	10 W in α-mode
Working gas, flow rate	Ar + 0.05–1% H_2O, 2 slm
Pumping laser	SpectraPhysics INDI
	YAG:Nd
Dye laser	Sirah Cobra Stretch
Dye solution, wavelength	Rhodamine 590, 283.463 nm
Laser energy for LIF	34 μJ
Laser line-width, frequency	0.03 cm^{-1}, 10 Hz
Laser pulse duration	4 ns
(FWHM)	(Gaussian profile)
Photon counter, bin-width	SR430, 5 ns
Spectrometer, resolution	Shamrock 750, 0.03 nm
ICCD camera, gate time	AndoriStar 740, 50 ns
Detection volume of LIF	$V_f = 1.6 \times 10^{-9}$ m^3
Rayleigh scattering	$n_{air} = 1.95 \times 10^{25}$ m^{-3}
	$\sigma_{\lambda_R} = 7.6 \times 10^{-30}$ m^{2*}
	$V_R = 8.75 \times 10^{-9}$ m^3
	$W_L = 0.91$ J m^{-2}

* The value is taken from reference [17].

where η_c is the collection efficiency of the LIF detection system, Ω_f and V_f are the detection solid angle [sr] and the observation volume [m^3], $t(\lambda_{ij})$ and $G(\lambda_{ij})$ are the filter transmittance and the photomultiplier sensitivity for the OH emission wavelength corresponding to transition from upper level i to lower level j (in which i and j respectively stand for the upper level $n'v'J'$ of $OH(A)$ and the lower level $n''v''J''$ of $OH(X)$, with n, v, J the electronic, vibrational, and rotational quantum numbers). $\varepsilon_{ij}(t)$ is the wavelength integrated emission coefficient [W m^{-3} sr^{-1}] at moment t, which is defined by

$$\varepsilon_{ij}(t) = \int \frac{1}{4\pi} A_{ij} E_{ij} n_i(t) \varphi(\lambda_{ij}, t)\, d\lambda \tag{2}$$

where A_{ij} is the transition probability [s^{-1}], E_{ij} is the energy gap [J] of the corresponding transition, $n_i(t)$ is the density [m^{-3}] of the upper level at moment t, and $\varphi(\lambda_{ij}, t)$ is the spectral profile of the emission line of interest, for which counts that $\int \varphi(\lambda)d\lambda = 1$. From the Rayleigh scattering calibration, the sum $\sum[t(\lambda_{ij})G(\lambda_{ij})\int_0^t \varepsilon_{ij}(t)dt]$ in equation (1) can be obtained and expressed in absolute units in order to calibrate the experimental LIF signal. The Rayleigh scattering intensity I_R can be approximated

by [8,20]

$$I_R = \int_0^t I_R\left(\lambda_R, t\right) dt$$
$$= \eta_c t(\lambda_R) G(\lambda_R) \Omega_R V_R n_R [\sigma_{\lambda_R} K_{\lambda_R}(\theta) W_L] \quad (3)$$

where n_R is the scattering species density, σ_{λ_R} is the Rayleigh scattering cross section [m^2], $K_{\lambda_R}(\theta)$ is $3/8\pi$ for noble gases in the case of $90°$ observation [8], which was used here for Rayleigh scattering of air. W_L is the time-integrated energy density [$J\,m^{-2}$]. As the detection arrangements are the same for both LIF and Rayleigh scattering measurements, we can get

$$\sum \left[t\left(\lambda_{ij}\right) G(\lambda_{ij}) \int_0^t \varepsilon_{ij}\left(t\right) dt \right]$$
$$= t\left(\lambda_R\right) G\left(\lambda_R\right) n_R \left[\sigma_{\lambda_R} K_{\lambda_R}(\theta) W_L\right] \frac{V_R}{V_f} \frac{I_f^m}{I_R^m} \quad (4)$$

I_f^m and I_R^m are the time-integrated intensity of the measured LIF and Rayleigh scattering signals, respectively. Here we call the laser-pumped lower level of OH (X) level 1, the laser-excited upper level of OH (A) level 2, and we select one transition from level 2 to another lower level of OH (X), noted as level 3. Finally the time-integrated population of the laser-excited level $\int_0^t n_2(t)dt$ can be obtained from the calibrated sum of the emission coefficient:

$$\int_0^t n_2(t)dt = \alpha_{23} \frac{\sum \left[t(\lambda_{ij}) G(\lambda_{ij}) \int_0^t \varepsilon_{ij}\left(t\right) dt \right]}{t(\lambda_{23}) G(\lambda_{23})} \frac{4\pi}{A_{23} E_{23}} \quad (5)$$

where α_{23} is the fraction of the fluorescence intensity of transition $2 \to 3$ in the total generated LIF signals (filtered after narrow band filter and PMT). This fraction has been obtained from LASKIN simulation, but, in principle, can be calculated independently based on simulation of the LIF spectra.

Furthermore, the pumping from level 1 to level 2 by laser irradiation, and the loss of level 2 by different competing processes, can be described by

$$\frac{d}{dt} \frac{n_1(t)}{g_1} = -B_{12} W_L \frac{n_1(t)}{g_1} + \sum_{i \neq 1} Q_i^{RET} \frac{n_i}{g_i}$$
$$+ (A_{21} + B_{21} W_L) \frac{n_2(t)}{g_2} \quad (6)$$

$$\frac{d}{dt} \frac{n_2(t)}{g_2} = B_{12} W_L \frac{n_1(t)}{g_1} - (\Gamma_2 + B_{21} W_L) \frac{n_2(t)}{g_2} \quad (7)$$

where g_i and B_{ij} are the statistical weight of level i and the Einstein coefficient $i \to j$, Q_i^{RET} is the RET rate from all other rotational levels of OH (X) to level 1. Γ_2 is the total loss rate of level 2 without laser-stimulated emission, which includes rates of pre-dissociation, quenching, spontaneous emission, RET and VET processes. Due to the fast RET process ($Q_i^{RET} \sim 10^9$ s^{-1}) [21], level 1 will be refilled rapidly because of the laser pumping and the number
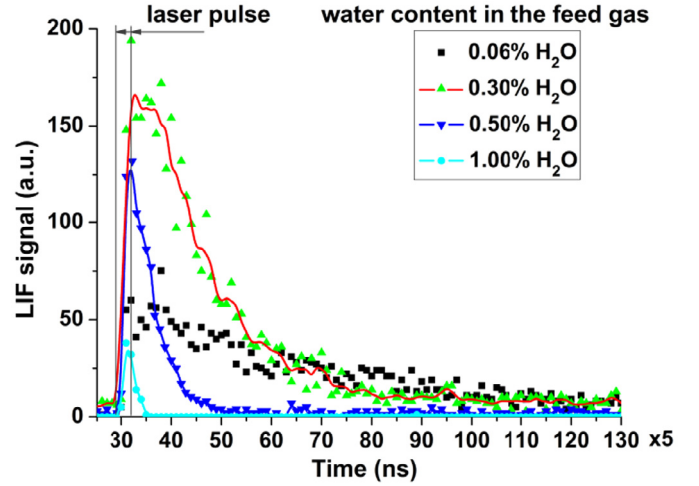

Fig. 3. (Color online) Typical time-resolved LIF signals of the OH radical at different water contents after excitation of P$_1$(4) transition.

density $n_1(t)$ can be approximated as constant $n_1(t) \sim n_1$ during the laser pulse. In our experiment $\frac{B_{21} W_L}{\Gamma_2} \sim 10^{-2}$, so we can simplify:

$$n_2(t) = \begin{cases} \frac{g_2}{g_1} \frac{B_{12} W_L}{\Gamma_2} n_1 \left[1 - \exp\left(-\Gamma_2 t\right)\right] & t < \tau \\ n_2(\tau) \exp\left[-\Gamma_2\left(t - \tau\right)\right] & t > \tau \end{cases} \quad (8)$$

where τ is the laser pulse duration with $\tau \sim 10$ ns. Based on $\int_0^t n_2(t)dt$, determined from equations (5) and (8), the density n_1 of lower level 1 is estimated and applied to calculate the absolute concentration of ground state OH (X), based on the Boltzmann distribution:

$$N = n_1 \frac{\sum g_i \exp(-E_i / k_b T_r)}{g_1 \exp(-E_1 / k_b T_r)} \quad (9)$$

where E_i is the energy of level i, k_b is the Boltzmann constant and T_{rot} is the rotational temperature of OH (X).

4 Results and discussion

Typical time resolved LIF signals for the Ar RF jet discharge are presented in Figure 3 for the case of excitation of the P$_1$ (4) transition for different water contents at the position $z = 0.5$ mm above the nozzle. It is found that a highest LIF signal was observed with the mixture of Ar + 0.3% H$_2$O. The increase of the water content results in a significant drop of the peak intensity of the LIF signal and also in the decrease of the decay time due to strong quenching of the excited-state OH (A) by H$_2$O.

The model described above was applied to calculate the absolute OH density for the case of 0.3% H$_2$O admixture. A characteristic decay time about 74 ns (time resolution of detection system is 5 ns) was observed for the OH LIF signal under the experimental conditions, as shown in Figure 4. The fast decay of the LIF signal, which is much shorter than the radiative lifetime of excited OH
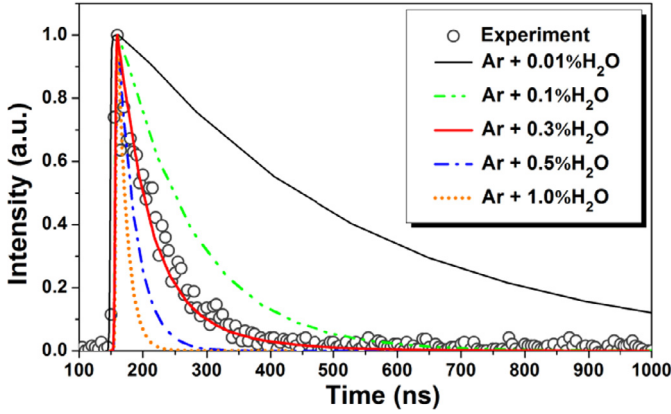
Fig. 4. (Color online) Decay fitting of experimental OH LIF signal by simulation results with different $H_2O\%$ admixtures. All the experiment and simulation signals are normalized. The water vapor percentage for the experiment is 0.3%, detected position $z = 1.0$ mm.
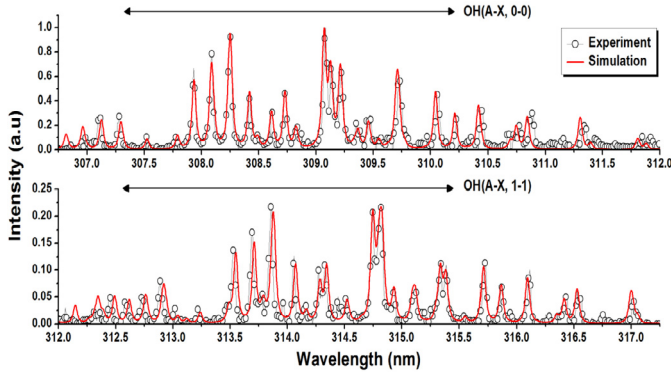

Fig. 5. (Color online) Comparison of the experiment and simulation LIF spectrum of OH (A-X, 0-0) and OH (A-X, 1-1) emission bands. Intensities are normalized to the peak at 309 nm.

Table 2. Parameters of the transitions of OH (A-X) used in the calculation model.

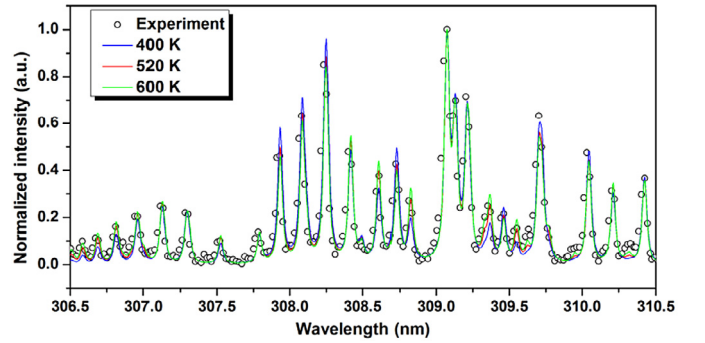| Transitions	λ	$E_{v''J''}^{v'J'}$	$A_{v''J''}^{v'J'}$	$B_{v'J'}^{v''J''}$
OH (A, $v' = 1$, $J' = 3$) $\rightarrow$	(nm)	(cm^{-1})	(s^{-1})	$(m^2\,J^{-1}\,s^{-1})$
Excitation transition				
OH (X, $v'' = 0$, $J'' = 4$)	283.4	35278	1.44E+05	5.29E+08
LIF transitions				
OH (X, $v'' = 1$, $J'' = 4$)	315.2	31721	2.72E+05	1.37E+09
OH (X, $v'' = 1$, $J'' = 3$)	313.8	31868	3.37E+05	2.10E+09
OH (X, $v'' = 1$, $J'' = 2$)	312.7	31983	0.82E+05	6.72E+08

Fig. 6. (Color online) Spectrum fitting of the rovibrational band of OH (A-X, 0-0) by synthetic simulation spectra at different rotational temperatures. The water admixture is 0.3%.

levels (700–1100 ns depending on the transition) [22], was attributed to the quenching of excited OH radicals by different species (H_2O, Ar, H, etc.) in the atmospheric pressure plasma environment [23]. Under our experimental conditions, water vapor is considered as the dominant quencher for excited OH (A) [5,21]. The quenching effects on OH (A) levels by H_2O are demonstrated clearly from the simulated LIF decay fitting with different $H_2O\%$ admixtures shown in Figure 4. In the LIF simulation, the effects of air molecules due to diffusion were ignored and only the two background gas species, i.e. Ar and H_2O, were considered. It is a reasonable approximation because the main part of the LIF signal is coming from the core of the jet where back-diffusion of the air is negligible, especially for plasma volumes close to the gas outlet.

As we can see, the best fitting with the 0.3% H_2O mixture agrees well with the experimental condition. Further agreement was proven by comparing the LIF spectrum simulation of OH (A-X, 0-0) and OH (A-X, 1-1) emission bands to the experimental one, as shown in Figure 5.

The spectrum presented in Figure 5 was recorded immediately after the laser pulse with an ICCD exposure time of 50 ns. We have to emphasized that initially the

state OH (A, $v' = 1$) was excited but strong fluorescence intensity from OH (A-X, 0-0) in the experiment was observed as well. The appearance of OH (A-X, 0-0) is attributed to the important ro-vibrational processes. In the mixture of Ar + 0.3% H_2O, the VET transfer of OH (A) is mainly the result of collisions with argon atoms with a cross-section of 0.44 ± 0.06 Å^2 [24]. Based on the simulation results, the fraction of the fluorescence intensity from the laser-excited level OH (A, $v' = 1$, $J' = 3$) to a selected lower level of the OH (X, $v' = 1$) vibrational manifold in the total detected LIF intensity is acquired. Next, it is used in the calculation model to determine the density of the laser-pumping lower level OH (A, $v' = 0$, $J' = 4$). The reason the fluorescence transitions of OH (A-X, 1-0) and OH (A-X, 1-2) bands are not selected is because of the limited filter transmittance range of 10 nm with a maximum at 309 nm. A total loss rate $\Gamma_2 = 2.87 \times 10^{10}$ s^{-1} of the laser-excited level is found from simulation and applied in the model. In order to average the experimental results, three fluorescence lines of the OH (A-X, 1-1) bands are selected for the model calculation, as listed in Table 2 with their spectral parameters [29,35].

The estimated value of $\int_0^t n_2(t)dt$, see equation (5), allows us to calculate the ground density of OH through equations (8) and (9) where T_{rot} has been measured independently, e.g. by optical emission spectroscopy.

The emission spectrum has been measured at the same position $z = 1.0$ mm and presented in Figure 6. The simulation of the spectra has been done in the LIFbase

Table 3. OH densities in various plasma sources.

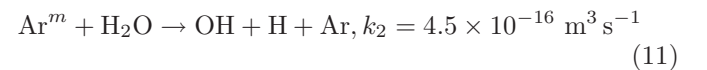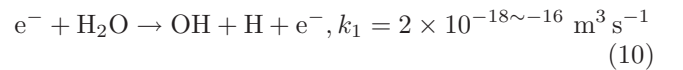| Source/Power [W]	OH density, [m^{-3}]	Method	Reference
MW jet in Ar/38 W	1.1×10^{22}	CRDS	[25]
DBD, He jet + 300 ppm H$_2$O/2.5 W	6×10^{19}	LIF	[28]
DBD, He + 6700 ppm H$_2$O	3.7×10^{19}	IR CRDS	[26]
Gliding arc in air	10^{20}	LIF	[32]
RF discharge, He + H$_2$O, up to 100 W	$6 \times 10^{19*} \div 4 \times 10^{20}$ active zone	UV absorption	[27]
RF jet Ar + 0.3% H$_2$O/10 W	$2.50 \times 10^{19*}$	LIF	Here

*Average value over 3 transitions.

program [35]. The rotational temperature 520 ± 50 K was estimated by fitting the experimental OH (A-X, 0-0) optical emission bands. Recently, it was shown that measurements of T_{rot} from OH emission can be incorrect at high water contents in the discharge because of the overpopulation of the OH (A) state at high rotational numbers, see [21] and references therein. But it is found that in RF plasma at 0.3% H$_2$O the one temperature fit gives good agreement with experimental data and no overpopulation of the OH (A) state has been observed at such a low content of H$_2$O. The good fitting of the OH band by a single rotational temperature simulation spectrum indicates that the rotational population distribution of OH (A) achieves equilibrium and follows the Boltzmann distribution function. The method applied in the present work gives a good convergence independently on transitions used for the calculation model. The absolute ground densities of OH radicals in the RF jet for 3 different detected transitions presented in Table 2 have been calculated as 2.71, 2.47 and 2.42×10^{19} m^{-3}, respectively. Such a good agreement is a clear advantage of the calculation method. The absolute ground density of OH radicals in the afterglow of the RF jet is presented in Table 3, where absolute OH densities in different high pressure plasmas measured by others are presented for comparison as well. In addition to LIF method, other techniques such as cavity ring-down spectroscopy (CRDS), infrared CRDS, and broadband UV absorption spectroscopy were applied to determine the OH concentrations in various atmospheric pressure plasma sources (as listed in Tab. 3). Based on the high-resolution CRDS, Wang and Srivastava [25] selected the ro-vibrational line R$_2$(4) for the line-shape measurement for the OH number density. Comprehensive characterization of OH generation of the microwave plasma jet operating at various working gases was reported. Similar measurements by using the near infrared continue wave CRDS at the P-branches of OH X$^2\Pi$ ($v'' = 0 \rightarrow v' = 2$) were reported by Liu et al. [26] to determine the OH concentrations in H$_2$O/He DBD plasmas. Compared to CRDS in UV region, operation in near infrared area has advantages of compact and inexpensive diode laser system, but disadvantages of relative weak line strengths of OH

spectrum. Recently, Bruggeman et al. [27] measured the OH density by the broadband UV absorption technique in a RF glow discharge. This method is similar to that of laser absorption spectroscopy using the Beer-Lambert law and requires the analysis of the absorption line shape. For all the details of these techniques can be found in references [25–28].

Unfortunately, up to now, the LIF data on OH (X) density in a cold RF Ar plasma jet are absent in literature. Available estimations in microwave Ar plasma jet give much higher OH density around 10^{22} m^{-3}. The big difference with the RF jet can be explained by the higher electron density and especially electron temperature in microwave plasmas [25] and by the higher input power. Other results presented in Table 3 for discharges in He/water mixtures show similar OH densities in those plasmas where the small difference can be explained by different input power and by the fact that discharge in He usually is characterized by higher electron temperature [5,23].

The OH radicals can be produced by a big number of mechanisms, which depends on the plasma properties. In low-temperature discharges with low ionization degree ($\sim 10^{-4}$) the OH production is primarily ascribed to be due to electrons and Ar metastables induced by dissociation of water vapour [5]. Two dominant mechanisms can be [29,30]:

$$e^- + H_2O \rightarrow OH + H + e^-, k_1 = 2 \times 10^{-18 \sim -16} \text{ m}^3 \text{ s}^{-1} \quad (10)$$

$$Ar^m + H_2O \rightarrow OH + H + Ar, k_2 = 4.5 \times 10^{-16} \text{ m}^3 \text{ s}^{-1} \quad (11)$$

where k_1 is estimated at typical conditions for low temperature jets, i.e. an electron temperature of 1–2 eV. The yield of OH (X) due to the second reaction obviously is a function of the Ar^m density. We estimated the argon metastable $1s_5$ state density by means of the resonant optical absorption spectroscopy using the 811.53 nm argon line. More details of the set-up can be found in [31], which is out of the scope of the present work. The spatial averaged Ar^m density is estimated to be 3×10^{17} m^{-3},

which is about two orders of magnitude lower than the OH (X) density, see Table 3. It indicates that the contribution of Ar^m to the OH (X) production is negligible in the afterglow of the RF plasma jet. At the same time, the electron number density, which affects electron dissociation of water molecules, can be estimated from the Stark broad-banding of the H_β line measured at the same position in the jet afterglow. The approximated calculation formula of the plasma electron density from the full-width at half-maximum (FWHM) of Stark broadening of the H_β line is [33]:

$$FWHM = 4.80 \text{ nm} \times \left(\frac{n_e}{10^{23} \text{ m}^{-3}} \right)^{0.68116}. \quad (12)$$

The Van der Waals broadening contribution to the FWHM of the Lorentzian component of the H_β line in nm is estimated by:

$$\Delta\lambda_V = \frac{A}{T_g^{0.7}} \quad (13)$$

where coefficient A is calculated to be 1.64 from Laux et al. [34]. The Doppler broadening in nm of the H_β line is calculated by:

$$\Delta\lambda_D = 3.48 \times 10^{-4} T_g^{0.5}. \quad (14)$$

The contribution of the natural broadening is very small compared to other broadening mechanisms. For $T_g = 520$ K the calculated $\Delta\lambda_V$ and $\Delta\lambda_D$ are 0.02 nm and 0.008 nm, respectively. The instrumental function has a Lorentzian shape with FWHM of 0.048 nm, which is obtained by using a low-pressure Hg lamp. The Doppler broadening is very weak compared to the instrumental, Van der Waals, and Stark broadenings, which leads to an almost Lorentzian profile for the measured H_β line, as shown in Figure 7. The FWHM of Stark broadening is obtained by subtracting the instrumental FWHM and $\lambda\Delta_V$ from the measured FWHM. An average electron density of 2.8×10^{19} m^{-3} is obtained at the position $z = 1.0$ mm in the jet afterglow. The electron density is in the same range with the OH concentration, which points out the dominant role of the mechanism of electron-collision induced H_2O dissociation in the OH generation by reaction (11).

5 Conclusions

In conclusion, an improved calculation method to determine the absolute density of ground state OH radicals is proposed for LIF measurements. Various energy transfer processes (radiative transitions, quenching, predissociation, rotational and vibrational energy transfer) between OH (A) radicals and colliders in plasma are considered. An absolute OH density of 2.50×10^{19} m^{-3} is calculated in the afterglow of an atmospheric pressure RF plasma jet operating with Ar + 0.3% H_2O mixtures. It is found that the OH production is dominated by the dissociation process of H_2O induced by electron collisions in the discharge. Generation of OH (X) due to the dissociative reaction of H_2O by Ar metastables plays a negligible role because of the low density of metastables around 3×10^{17} m^{-3}.
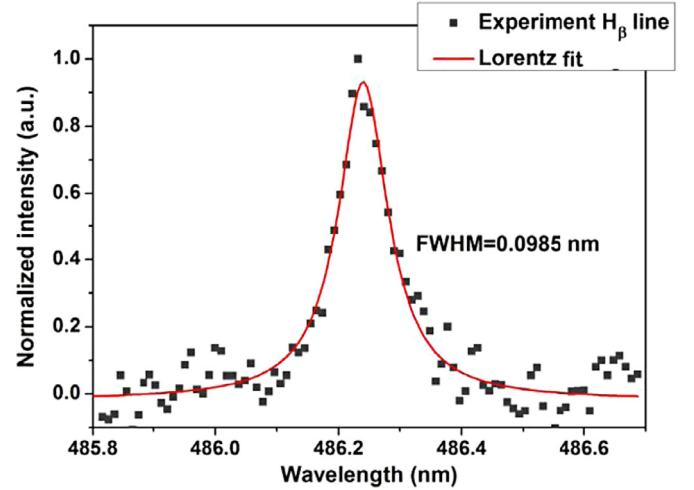

Fig. 7. (Color online) Lorentz fit of the experimental H_β line from the Ar + 0.3% H_2O RF plasma jet.

References

1. J. Chunqi, A.A.H. Mohamed, R.H. Stark, J.H. Yuan, K.H. Schoenbach, IEEE. Trans. Plasma Sci. **33**, 1416 (2005)
2. R. Rudolph, K.P. Francke, H. Miessner, Plasma Chem. Plasma Process. **22**, 401 (2002)
3. C.M. Marks, L.D. Schmidt, Chem. Phys. Lett. **178**, 358 (1991)
4. M.A. Malik, Plasma Chem. Plasma Process. **30**, 21 (2009)
5. P. Bruggeman, D.C. Schram, Plasma Sources Sci. Technol. **19**, 045025 (2010)
6. R. Ono, T. Oda, IEEE. Trans. Ind. Appl. **37**, 709 (2001)
7. G. Dilecce, P.F. Ambrico, M. Simek, S. De Benedictis, Appl. Phys. B **75**, 131 (2002)
8. H.F. Döbele, T. Mosbach, K. Niemi, V.S. von der Gathen, Plasma Sources Sci. Technol. **14**, S31 (2005)
9. R. Kienle, M.P. Lee, K. Kohse-Höinghaus, Appl. Phys. B **63**, 403 (1996)
10. A. Ershov, J. Borysow, J. Phys. D **28**, 68 (1995)
11. R. Ono, T. Oda, J. Phys. D **35**, 2133 (2002)
12. S. Yonemori, Y. Nakagawa, R. Ono, T. Oda, J. Phys. D **45**, 225202 (2012)
13. G. Dilecce, P.F. Ambrico, M. Simek, S. De Benedictis, Chem. Phys. **398**, 142 (2012)
14. F. Tochikubo, S. Uchida, T. Watanabe, Jpn J. Appl. Phys. **43**, 315 (2004)
15. T. Verreycken, R.M. van der Horst, A.H.F.M. Baede, E.M. van Veldhuizen, P.J. Bruggeman, J. Phys. D **45**, 045205 (2012)
16. F. Tochikubo, S. Uchida, T. Watanabe, Jpn J. Appl. Phys. **43**, 315 (2004)

17. R.B. Miles, W.R. Lempert, J.N. Forkey, Meas. Sci. Technol. **12**, R33 (2001)
18. U. Rahmann, A. Bulter, U. Lenhard, R. Dusing, D. Markus, A. Brockhinke, K. Kohse-Hoinghaus, *LASKIN – A Simulation Program for Time-Resolved LIF-Spectra*, Internal Report, University of Bielefeld, Faculty of Chemistry, Physical Chemistry
19. R. Kienle, M.P. Lee, K. Kohse-Höinghaus, Appl. Phys. B **62**, 583 (1996)
20. J.T. Salmon, N.M. Laurendeau, Appl. Opt. **24**, 65 (1985)
21. P. Bruggeman, F. Iza, P. Guns, D. Lauwers, M.G. Kong, Y.A. Gonzalvo, C. Leys, D.C. Schram, Plasma Sources Sci. Technol. **19**, 015016 (2010)
22. C.B. Cleveland, J.R. Wiesenfeld, Chem. Phys. Lett. **144**, 479 (1988)
23. P. Bruggeman, T. Verreycken, M.Á. González, J.L. Walsh, M.G. Kong, C. Leys, D.C. Schram, J. Phys. D **43**, 124005 (2010)
24. L.R. Williams, D.R. Crosley, J. Chem. Phys. **104**, 6507 (1996)
25. C. Wang, N. Srivastava, Eur. Phys. J. D **60**, 465 (2010)
26. Z.W. Liu, X.F. Yang, A.M. Zhu, G.L. Zhao, Y. Xu, Eur. Phys. J. D **48**, 365 (2008)
27. P. Bruggeman, G. Cunge, N. Sadeghi, Plasma Sources Sci. Technol. **21**, 035019 (2012)
28. S. Yonemori, Y. Nakagaw, R. Ono, T. Oda, J. Phys. D **45**, 225202 (2012)
29. Y. Itikawa, J. Phys. Chem. Ref. Data **34**, 1 (2005)
30. S. Novicki, J. Krenos, J. Chem. Phys. **89**, 7031 (1988)
31. N. Britun, M. Gaillard, Y.M. Kim, K.S. Kim, J.G. Han, Met. Mater. Int. **13**, 483 (2007)
32. B. Benstaali, P. Boubert, B.G. Cheron, A. Addou, J.L. Brisset, Plasma Chem. Plasma Process. **22**, 553 (2002)
33. M.A. Gigosos, M.A. Gonzalez, V. Cardenoso, Spectrochim. Acta Part B **58**, 1489 (2003)
34. C.O. Laux, T.G. Spence, C.H. Kruger, R.N. Zare, Plasma Sources Sci. Technol. **12**, 125 (2003)
35. J. Luque, D.R. Crosley, *LIFBASE: database and spectral simulation (version 1.5)* (1999)